Soil Biology and Biochemistry 184 (2023) 109097

Contents lists available at ScienceDirect

Soil Biology and Biochemistry

journal homepage: www.elsevier.com/locate/soilbio

Resolving dynamic mineral-organic interactions in the rhizosphere by combining in-situ microsensors with plant-soil reactive transport modeling

Mariela Garcia Arredondo [a,1], Yilin Fang [b,1], Morris Jones [c], Steve Yabusaki [b], Zoe Cardon [d], Marco Keiluweit [a,e,*]

[a] School of Earth & Sustainability and Stockbridge School of Agriculture, University of Massachusetts, Amherst, MA, USA
[b] Pacific Northwest National Laboratory, Earth Systems Science Division, Richland, WA, USA
[c] College of Health and Natural Sciences, Franklin Pierce University, Rindge, NH, USA
[d] Marine Biological Laboratory, The Ecosystems Center, Woods Hole, MA, USA
[e] Institute of Earth Surface Dynamics, University of Lausanne, Lausanne, Switzerland

ARTICLE INFO

Keywords:
Soil carbon
Rhizosphere
Mineral-organic associations
Mineral-associated organic matter
Diel cycles
Reactive transport modeling
Microsensors

ABSTRACT

Associations between minerals and organic matter represent one of the most important carbon storage mechanisms in soils. Plant roots are major sources of soil carbon, and resolving the dynamics and dominance of microbial consumption versus mineral sorption of root-derived carbon is critical to understanding soil carbon storage. Here we integrate *in-situ* rhizosphere microsensor and plant physiological measurements with a 3-D plant-soil reactive transport model to explore the fate of dissolved organic carbon (DOC) in the rhizosphere, particularly its microbial consumption and interaction with Fe oxide minerals. Over several days, microdialysis probes at the root-soil interface of growing *Vicia faba* roots in live soil, revealed clear diel patterns of DOC concentration in the pore water. Daytime DOC spikes coincided with peaks in leaf-level photosynthesis rates and were accompanied by declining redox potential and dissolved oxygen as well as increasing pH in the rhizosphere. Incorporating microsensor data into our modeling framework showed that the measured rapid loss of DOC after each mid-day spike could not be explained by consumption via aerobic respiration, nor via anaerobic respiration dominated by Fe oxide reduction. Rather, in the model, a large fraction of rhizosphere DOC was rapidly immobilized each day by adsorption to Fe oxides. Further, modeled microbial Fe reduction (fueled by DOC) did not mobilize significant organic carbon from Fe oxides during the day. Instead, the model predicted equilibrium desorption of organic carbon from Fe oxides at night. This new mechanistic modeling framework, which couples aboveground plant physiological measurements with non-destructive high-resolution monitoring of rhizosphere processes, has great potential for exploring the dynamics and balance of the various microbial reactions and mineral interactions controlling carbon storage in soils.

1. Introduction

Plants direct a large proportion of photosynthetically fixed carbon (C) to roots and the rhizosphere via sloughed-off root cells, secretions such as mucilage, and a variety of exuded organic compounds—known collectively as rhizodeposits (Kuzyakov and Domanski, 2000; Cheng and Gershenson, 2007). Rhizodeposition, and associated microbial biomass and products, are the primary sources of C in most soils, often promoting C accrual (Rasse et al., 2005; Clemmensen et al., 2013). Because root- and microbe-derived C is in intimate contact with the surrounding mineral matrix, it may form mineral-organic associations (MOAs) that withstand microbial attack (e.g., Schmidt et al., 2011). However, recent evidence suggests that rhizodeposition may liberate C bound to protective minerals, enhancing microbial access, and causing a loss of previously protected C (Keiluweit et al., 2015; Li et al., 2021). To better predict under what circumstances plant roots promote C accrual or loss from soil, an improved mechanistic understanding of the fate of rhizodeposits and mineral-organic associations in the rhizosphere is needed.

Although MOAs are principal C storage mechanisms and are generally assumed to be relatively stable, recent evidence suggests MOAs are

* Corresponding author. .Institute of Earth Surface Dynamics, University of Lausanne, Lausanne, Switzerland.
E-mail address: marco.keiluweit@unil.ch (M. Keiluweit).
[1] both authors contributed equally.

https://doi.org/10.1016/j.soilbio.2023.109097
Received 4 March 2023; Received in revised form 7 June 2023; Accepted 11 June 2023
Available online 24 June 2023

dynamically transformed in the rhizosphere, with largely unknown consequences for the fate of soil C. For example, while Neurath et al. (2021) showed rapid and mineral-dependent accumulation of rhizodeposits on mineral surfaces such as Fe and Al oxides, they also suggest dynamic exchange between mineral-associated and accessible pools. This dynamic exchange may be because root activity does not merely introduce "carbon" to the rhizosphere. Roots manipulate ligand concentration, fuel microbial activity, alter pH/E_H conditions, and drive water flow in the rhizosphere, thereby inducing biogeochemical changes with the potential to undermine the stability of MOAs. For example, the common exudate oxalic acid, acting as a ligand, can effectively destabilize MOAs by dissolving Fe and Al oxides (Keiluweit et al., 2015; Li et al., 2021). Moreover, the release of energy-rich exudates can stimulate microbial O_2 consumption to create transient anaerobic microsites conducive to the reductive dissolution of Fe oxides (Fischer et al., 1989). Roots are also well known to alter pH, which affects the solubility and surface charge of Fe and Al oxides (Thompson et al., 2006; Marinos and Bernhardt, 2018), mobilizing organic matter (Marinos and Bernhardt, 2018; Bailey et al., 2019). Finally, diel cycles in plant transpiration drive oscillating soil moisture in the rhizosphere (Cardon and Gage, 2006), resulting in drying and wetting cycles potentially altering sorption equilibria (Espeleta et al., 2017) and redox potential (E_H) (Fischer et al., 1989; Calabrese and Porporato, 2019) that could control the stability of MOAs and even influence mineral precipitation. Such rhizosphere processes regulate the formation and disruption of MOAs over long-time scales (Garcia Arredondo et al., 2019), but the underlying mechanisms in dynamic rhizosphere environments remain poorly resolved.

A new generation of mechanistic plant-soil models are particularly promising tools to explore and predict links between plant physiology and belowground biogeochemistry, including possible impacts on MOAs. For maximum impact, small-scale experimental data from plants and soils of known characteristics, measured nondestructively around roots over multiple days, should be combined with the rigorous stoichiometric and kinetic framework in reactive transport modeling. This measurement-model combination is ideally suited to explore the balances and dynamics of mechanisms affecting the fate of DOC, particularly its sorption to minerals and consumption by microbes. Here we use eSTOMP-ROOTS, which combines a root system architecture model (RootBox) and a reactive transport model (eSTOMP) (Fang et al., 2019). RootBox simulates 3-D root growth and architecture using a Lindenmayer System (L-systems) (Leitner et al., 2010a; 2010b; Schnepf et al., 2018). eSTOMP, is a variably saturated flow and geochemical multicomponent reactive transport model (Yabusaki et al., 2011), which represents explicit chemical reactions such as microbial respiration, sorption/desorption, and mineral dissolution. The cintegration of these models offers the opportunity to simulate the cascading effects of altered plant physiology (e.g., as induced by climate or nutrient stressors) on rhizodeposition, resultant rhizosphere biogeochemistry and, ultimately, formation and destabilization of MOAs.

To take advantage of this opportunity also requires that sufficient empirical information be available to parameterize and/or constrain a mechanistic plant-soil model such as eSTOMP-ROOTS. Ideally, one would combine plant physiological measurements (i.e., photosynthesis, transpiration) with concurrent, nondestructive measurements of rhizosphere biogeochemical parameters such as rhizosphere DOC pool size, pH and E_H changes, and solute concentrations. While aboveground measurements of photosynthesis and transpiration are relatively straightforward, nondestructive biogeochemical measurements in the rhizosphere are challenging and require high spatial and temporal resolution. Previous observations indicate that, in some cases, exudation (McDougall and Rovira, 1970; Dennis et al., 2010), microbial activity (Herron et al., 2013), and pH or E_H (Fischer et al., 1989) change within hourly timescales and along micrometer-scale gradients around individual roots. Microsensors hold significant promises for capturing such dynamics. Microdialysis probes are capable of passively sampling pore water solutes at sub-mm-scales (Inselsbacher et al., 2011), and have been used to probe rhizosphere solutes (Brackin et al., 2017). Voltametric and potentiometric microelectrodes can resolve pH, E_H, and dissolved oxygen (DO) dynamics in the rhizosphere (Dai et al., 2022).

Here, our objective was to develop a mechanistic framework for exploring the fate of root-derived C, specifically its sorption to minerals and microbial consumption, in the rhizosphere. We (i) quantified short-term variations in rhizosphere biogeochemistry using a novel microsensor array, linked those data with observations of leaf-level photosynthesis and transpiration, and incorporated the information into eSTOMP-ROOTS. The modeling structure (ii) provided the stoichiometric and kinetic framework for examining the fate of root-derived DOC, particularly its consumption by microbes and interaction with a common Fe oxide mineral (ferrihydrite). We used *Vicia faba* because of its agricultural relevance, its easily visible root system (Knott, 1990), and because of prior reports on its strong impact on pH and E_H dynamics in the rhizosphere (Fischer et al., 1989). We measured and modeled rhizosphere system behavior over five diel cycles because we expected daily variation in photosynthesis and transpiration to drive distinct yet repetitive changes in rhizosphere biogeochemistry (Cardon and Gage, 2006; Espeleta et al., 2017). The combination of novel rhizosphere-scale measurements with reactive transport modeling provided new insights into the importance of minerals and microbes in regulating the fate of root-derived C.

2. Methods

2.1. Rhizobox experiments

Rhizobox materials and design. To enable biogeochemical measurements at the root-soil interface, a custom rhizobox was developed (Fig. 1). The rhizobox consisted of a machined polycarbonate frame and two transparent covers (front and back). The siding of the back plate contained side ports for microprobes (diameter = 1.6 mm). Two reference and counter microelectrode probes were inserted through the front plate, about 4 cm away from the side ports. The interior rhizobox volume is 10 cm × 30 cm x 0.2 cm (l x h x w) (Fig. SI-1) and, when filled with soil, allows for the growth of young roots that are visible through the clear front plate. Individual roots are guided to the microsensor array along the side of the rhizobox using gravity (Fig. 2).

Soil characteristics. A fertile grassland soil classified as fine-loamy, mixed, superactive Ustic Haplocryolls (Fox et al., 2022) was collected at a 15 cm depth at the Rocky Mountain Biological Laboratory (Gothic, CO). The soil was air-dried at 22 °C and sieved (2 mm). Extractions were performed using hydroxylamine to determine easily reducible Fe pools (Courchesne and Turmel, 2007) and dithionite-citrate-carbonate to determine total reducible Fe pools (Wagai and Mayer, 2007). Fe(II) content was determined using ferrozine assays on HCl extracts (Gibbs, 1979; Viollier et al., 2000). To determine DOC in the extracts, samples were analyzed by TOC (Shimadzu TOC-L CPH with an ASI-L, Shimadzu Scientific Inst., Columbia, MD, USA). Fe concentrations in the extracts were determined after acidification with 2% nitric acid by ICP-MS (Shimadzu ICPMS-2030, Shimadzu Scientific Inst., Columbia, MD, USA). Particle size distribution and extractable nutrients were determined using standard methods.

Rhizobox experiment. Soils were brought to 40% water holding capacity using tap water and packed into the rhizobox to achieve field bulk density (1.5 g cm^{-3}). A single *V. faba* (Windsour variety) seedling with a tap root of ~3 cm length was transferred into the rhizobox. Soil moisture was maintained using a cotton wick connected to an amber glass flask containing tap water placed along the side of the rhizobox. The polycarbonate portions of the rhizobox were covered with aluminum foil to limit light exposure, leaving the top open for the plant to grow, and placed in a rack where it was held at a 30° angle to facilitate plant root growth along the sensor array. Rhizoboxes were maintained in a growth chamber set to 16 h light and 8 h dark cycle with a maximum of 500 μmol photons m^{-2} s^{-1} at 20% humidity for light hour settings and 25 °C

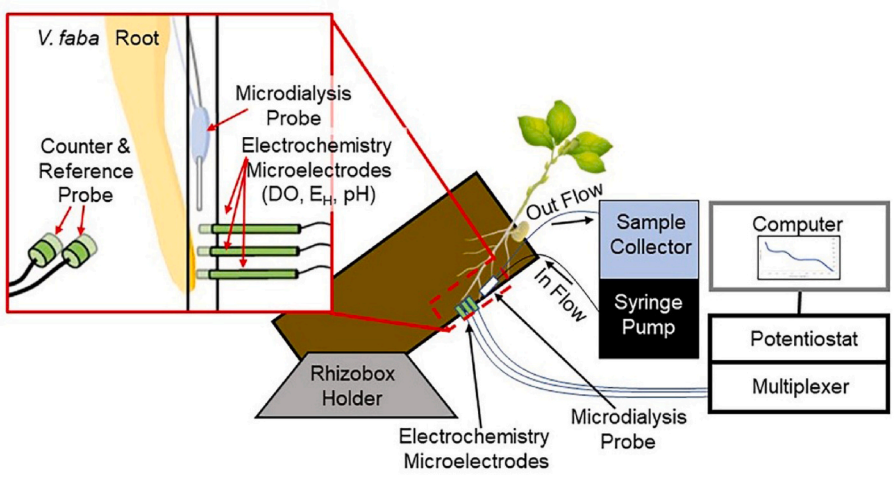

Fig. 1. Rhizobox and associated microsensor setup. Magnified panel shows microsensor array containing microelectrodes controlled by the potentiostat as well as microdialysis probe connected to water pump and fraction collector. Rhizoboxes are tilted at an angle of 30° degrees to facilitate root growth over the microsensor array. Detailed rhizobox design and dimensions included found in Figs. SI–1.

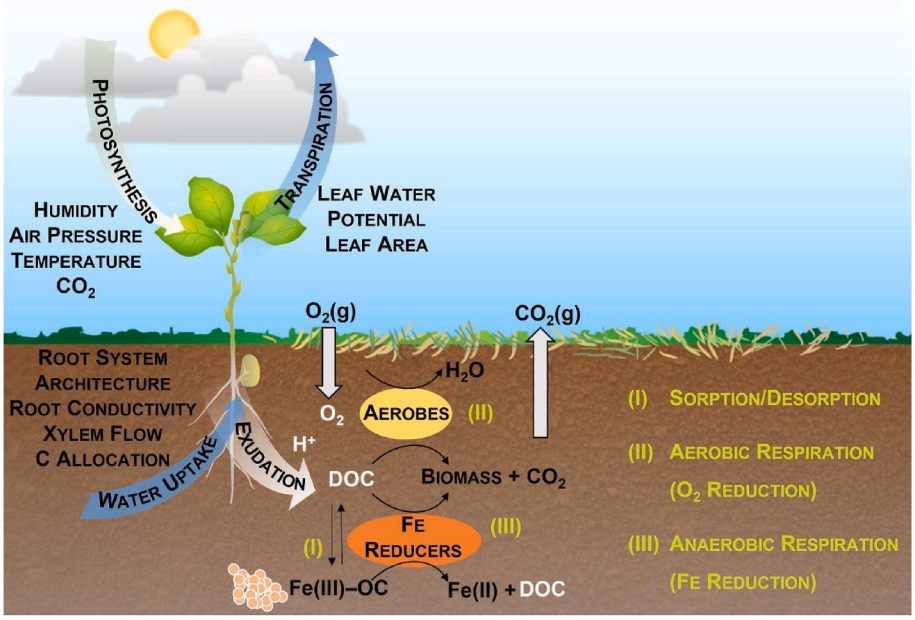

Fig. 2. Conceptualization of the biogeochemical reactions included in the numerical model to capture the measured diel dynamics in the rhizosphere. Rhizosphere biogeochemical parameters directly measured using microsensors are shown in white. Specific reactions incorporated into multicomponent reaction transport model (i.e., eSTOMP) are shown in yellow. We assumed that, during light periods (daytime), photosynthetic and transpiration activity are at their highest, causing high water uptake and exudation rates at the root-soil surface. Root exudates would increase DOC concentrations, with DOC being subject to microbial consumption (via respiration) and sorption to minerals. Microbial consumption of DOC was expected to lead to declines in DO and thus E_H. Declines in E_H and DO were assumed to lead to declines in aerobic respiration and relative to anaerobic respiration (Fe(III) oxide reduction). We anticipated that Fe(III) oxide reduction would re-mobilize Fe-bound OC.

light cycle temperature and 15 °C dark cycle temperature (Tables SI–1c). Plants entered the second nodal stage by the time their roots arrived at sensor array within the rhizoboxes.

Microelectrodes. Microelectrodes for pH, E_H, and DO concentration measurements were installed along the side port along which single roots were channeled and were constructed in-house within 1/16" PEEK™ tubing. pH microelectrodes were designed with modifications from Perley (1939). These were calibrated versus a Saturated Calomel Electrode or solid-state Ag/AgCl electrode in pH buffers. Microprobe redox electrodes were built following previous reporting in Vepraskas (2002) with modifications to fit the rhizobox side ports (Figs. SI–1). Changes in DO were monitored using solid Hg/Au voltametric microelectrodes. Hg/Au microelectrodes were constructed as previously reported in the literature (Luther et al., 2008) and used with stationary Ag/AgCl reference and platinum (Pt) counter electrodes. All measurements were made with a DLK-70 potentiostat (Analytical Instruments Systems, Ringoes, NJ) laboratory electrochemical analyzer which communicated via standard web browser on a laboratory laptop positioned outside of the growth chamber with connector cables extending outside from the analyzer to the micro-electrodes inside the rhizobox within the growth chamber. DO was quantified by linear sweep voltammetry (LSV), between −0.1 and −1.9 V at a scan rate of 100 mV s^{-1} with 10s of deposition at −0.1 V. For DO, a two-point calibration was conducted using oxygen-saturated NaCl saline (20 mM) water (100% saturation) and a deoxygenated NaCl saline (20 mM) water (0% saturation). To maintain reproducibility during analysis, the Au/Hg amalgam electrodes ran cyclic voltammetry before each LSV scan. The redox and pH probes were similarly maintained by running initial scans before collecting stable final data points at each time step in the experiments.

Microdialysis of dissolved organic carbon (DOC). Along the interior wall of each individual rhizobox, a 10 mm long microdialysis probe (CMA 20 Harvard Apparatus) was installed. The positioning of the microdialysis probe allowed continuous measurements of the root-soil interface along individual roots. Because the soft original tubing for the microdialysis was noticeably leaking DOC, the original soft tubing

was removed and replaced by more inert tubing (PEEK™, 0.65 mm OD x 0.12 mm ID, Sigma-Aldrich). This tubing fed into a fraction collector (CMA 142 Fraction Collector Harvard Apparatus, Hollister, MA) with previously sterilized capped glass vials that allowed for the collection of 300 μL h^{-1} per rhizobox. Ultrapure water was pumped through 10 mL airtight glass syringes to the microdialysis system by an auto-pump (Standard Infuse/Withdraw PHD, 2000 Syringe Pump, Harvard Apparatus, Hollister, MA). These syringes had three-port microvalves attached that were fastened to the ends of the PEEK™ tubing to the microdialysis system. The microdialysis tubing once affixed to the rhizobox was flushed with ultrapure water for 24 h. Once placed inside the growth chamber, rhizoboxes and microdialysis system were allowed to equilibrate for at least 24 h to adjust from soil rewetting after seedlings were transplanted into the rhizobox system. Once the tap root emerged approximately 1 cm from the top of the microdialysis probe, sampling was initiated to collect background soil pore water. Sampling continued as the root reached the probe, slowly growing along its surface. Samples were collected hourly (300 μL h^{-1}) and subsequently combined to provide composite samples of 4-h resolution. Composites were split, with half flash frozen and the other half refrigerated for immediate DOC analysis. Microdialysis sampling was conducted over three days whereas microelectrode measurements were conducted over five days. DOC concentrations were analyzed using the TOC-L/V- liquid manual small-volume sample injection unit for the total organic carbon analyzer (Shimadzu TOC-L CPH with an ASI-L, Shimadzu Scientific Inst., Columbia, MD, USA) with a glass airtight syringe following Stubbins and Dittmar (2012). Sample aliquots of 100 μL were manually injected and found to provide the best accuracy and precision with the smallest sample volume.

Plant Physiology, Photosynthesis and Transpiration. Photosynthesis and transpiration rates were measured on four replicate rhizoboxes treated identically to those described above. Measurements were taken on leaves on the second node using a LiCOR 6400XT gas exchange system (LI-COR Biosciences, Lincoln, NE) and leaf internal concentration (c_i between 221 and 248 μmol CO_2 mol^{-1} in the day) provided by a blue/red LED light source, temperature-controlled leaf cuvette set to 25 °C and light levels at 500 P AR, with an atmospheric CO_2 buffer attached (tubing attached to LiCOR 6400XT that fed into 20 L carboy). Measurements were taken over a 24-hr period and recorded every 5 min to record diel plant responses in photosynthesis, stomatal conductance, and transpiration. In addition, we collected leaf area and leaf count from *V. faba* at the second node stage. This information was used to parameterize photosynthetic and transpiration rates for the entire plant system in the model.

2.2. 3-D mechanistic plant-soil model

We used the data collected as described above to build a rhizosphere biogeochemistry model based on eSTOMP-ROOTS (Fang et al., 2019) to determine the fate of newly produced DOC and examine the ensuing dynamics on mineral-organic associations. eSTOMP-ROOTS is unique in that it combines plant biophysical data and a root architecture model with a flow and reactive transport model, providing a platform to mechanistically explore how plant activity affects rhizosphere hydro-biogeochemistry. The following describes the implementation of photosynthesis, transpiration, water transport, root growth, root exudation, and soil biogeochemical processes of interest in the model (Fig. 2), with reactions and rate parameters summarized in Tables 1 and 2. Model simulations were initiated at t = 8 h to match the beginning of the first light period.

Root architecture. The root system architecture (RSA) model RootBox was parametrized using the dicot template from RootBox to mimic the second node stage (early vegetative stage) of *V. faba* (Knott, 1990). To directly compare our empirical results measured along a single root tip to model outputs, we established root system architecture comparable to that within the rhizoboxes. The size of the simulated rhizobox is 10 cm × 24 cm × 0.2 cm to accommodate the pre-generated root system. The root radius was set to 0.5 mm and the depth of the tap root is 17.2 cm below the top. The root geometry is shown in Fig. SI-2. Rhizosphere biogeochemistry throughout the entire root system was modeled, but modeling results for the deepest secondary root tip were used for comparisons to the measurements. However, plant growth and root architecture were assumed to be static over the experimental period.

Table 1
Equilibrium reaction and thermodynamic parameters.

Equilibrium Reaction	Log K	Function
$2\,H^+ + CO_3^{2-} = H_2CO_3$	16.68	Proton balance
$H^+ + CO_3^{2-} = HCO_3^-$	10.33	Proton balance
$Fe^{2+} + H_2O{=}H^+ + FeOH^+$	−9.5	Fe(II) hydrolysis
$CH_3COO^- + Fe^{2+} = FeCH_3COO^+$	1.82	Fe(II) complexation
$Fe^{2+} + CO_3^{2-} + H^+ = FeHCO_3^-$	12.33	Ferrous carbonate complexation
$Fe^{2+} + CO_3^{2-} = FeCO_3(aq)$	5.5	Ferrous carbonate complexation
$Fe^{2+} + 2\,CO_3^{2-} = Fe(CO_3)^{2-}$	7.1	Ferrous carbonate complexation
$CH_3COO^- + FeOOH(s) =$ Fe–C	Modified Langmuir isotherm in Eq. (1)	Equilibrium sorption

Table 2
Kinetic reaction, rate formulations, and rate parameters.

Kinetic Reaction	Rate formulation	Rate parameters	Function
a) $0.125\,CH_3COO^- + 0.6\,FeOOH(s) + 1.155\,H^+ + 0.02\,NH_4^+ = 0.02\,C_5H_7O_2N + 0.6\,Fe^{2+} + 0.96\,H_2O + 0.15\,HCO_3^-$			
	$r = k[FeOOH][DOC]$	$k = 0.0075$ $mol^{-1}\,L^{-1}\,d^{-1}$	Anaerobic respiration (Fe reduction)
b) $0.125\,CH_3COO^- + 0.1046\,O_2\,(aq) + 0.0291\,NH_4^+ = 0.0291\,C_5H_7O_2N + 0.0872\,H_2O + 0.0087\,H^+ + 0.1046\,HCO_3^-$			
	$r = k\frac{[O_2]}{K_d + [O_2]}\frac{[DOC]}{K_a + [DOC]}$	$k = 60$ μmol L^{-1} d^{-1} $K_a = 20$ μmol L^{-1} $K_d = 100$ μmol L^{-1}	Aerobic respiration (O_2 reduction)
c) $CH_3COO^- + FeOOH(s) =$ Fe–C			
	$r = k\,[DOC]$	$k = 70$ mol^{-1} L d^{-1}	Kinetic sorption (irreversible)

Water transport. Rhizosphere flow and reactive transport was simulated using a 3-D flow and reactive transport model, eSTOMP (extreme-scale Subsurface Transport Over Multiple Phases) (Yabusaki et al., 2011). eSTOMP solves variably saturated subsurface flow and multicomponent, reactive transport on massively parallel processing computers. It has recently been modified to simulate root water uptake (Fang et al., 2019) following the approach in Javaux et al. (2008) and Leitner et al. (2014) assuming negligible osmotic potential and root water capacitance.

The soil porosity and bulk density were 0.423 and 1530 kg m^{-3}, respectively. Based on soil texture (Carsel and Parrish, 1988), van Genuchten water retention function parameters α and m were 3.6 m^{-1} and 1.56, respectively, and hydraulic conductivity is 25 cm d^{-1} (0.25 m d^{-1}).

Soil water was initially in equilibrium with a constant water potential of −0.09 mH_2O (8.83×10^{-4} MPa) at the bottom and the four lateral sides of the model domain to simulate the soil moisture maintained during the experiment. The boundary conditions are constant throughout the simulation allowing water from the boundaries to generally replenish water taken up by the roots. A 24 h transpiration cycle with 41 mL d^{-1} based on our measurements of leaf area and use of a LiCOR 6400XT gas exchange system during the light period and 0.0

mL d^{-1} during the dark period is repeated at the root collar during the simulation period (110 h).

Root exudation. The input of DOC through root exudation was assumed to be located near each root tip (Fig. SI-2) consistent with empirical observations (Dennis et al., 2010). The flux of DOC released by the root tip was directly coupled to photosynthetically fixed C (Nguyen 2003; Kuzyakov and Domanski, 2000). Plant carbon allocation from these new photosynthates to roots was assumed to be instantaneous during each light period and evenly distributed among the roots. The portion of photosynthates released as root-derived DOC (exudates) was derived from previously measured photosynthetic rates, assuming root exudation represents no more than 40% of the photosynthetically fixed C (Nguyen 2003; Kuzyakov and Domanski, 2000). Both rate and timing of root exudation were adjusted (by trial and error) to match the measured rhizosphere DOC concentration values in the rhizosphere. Root-derived DOC is represented as acetate in the model, a weak organic acid, one of several classes of low molecular weight compounds released by roots (Jones and Darrah, 1994). Acetate was chosen because it is a dominant organic acid in the rhizosphere of *V. faba* (Saarnio et al., 2004; Lo Presti et al., 2021), and can act as both microbial substrate and sorbate to minerals (Hayakawa et al., 2018).

Adsorption and Desorption. Ferrihydrite (FeOOH) was chosen to represent easily-reducible Fe(III) oxides extracted by hydroxylamine (Tables SI–1b). The total ferrihydrite content was chosen based on the hydroxylamine-extractable amount and will hereafter be referred to as Fe(III) oxides. To represent reversible equilibrium sorption to these Fe (III) oxides in the model, we adopted a modified Langmuir model shown in Equations (1) and (2) proposed in Gu et al. (1994,1995) that describes adsorption and desorption of DOC on Fe(III) oxides:

$$q = \frac{K_{(q)} q_{max} DOC}{K_{(q)} C + 1} \tag{1}$$

$$K_{(q)} = K e^{-2bq} \tag{2}$$

where q (mg C m^{-2}) is the adsorbed quantity of organic carbon, q_{max} (mg C m^{-2}) is the maximum adsorbed quantity of organic carbon, DOC (g C m^{-3}) is the dissolved organic carbon concentration, $K_{(q)}$ (m^3 g^{-1}) is the affinity parameter, and b (m^2 mg^{-1}) is a parameter related to the heterogeneity of absorbent surfaces and adsorbates (Gu et al., 1995). It defined a surface excess-dependent affinity parameter to account for a decreasing adsorption affinity with surface coverage due to the heterogeneity of DOC and adsorbent surfaces. We used parameters reported at pH 6.3 to describe the sorption equilibrium (q_{max} = 0.285 mg C m^{-2}, b = 3.5 m^2 mg^{-1}, K = 2.71 m^3 g^{-1}) and an Fe(III) oxide specific surface area of 10.1 m^2 g^{-1} from Gu et al. (1995). Implementation of equation (1) is solved to equilibrium through iterations. However, given the pH-dependency and kinetically limited hysteresis of this reaction, we performed tests using variables from Gu et al. (1995) and confirmed the consistency of our results (Fig. SI-3). To account for irreversible sorption to Fe(III) oxides commonly observed for DOC (Gu et al., 1994, 1995), particularly in the case of organic acids such as acetate (Van Hees et al., 2003), a first order irreversible reaction for DOC sorption to Fe(III) oxides was also included (Table 2).

Aerobic and anaerobic respiration. Aerobic microbial respiration (i.e., the conversion of DOC to CO_2 coupled to DO consumption) was modeled with dual Monod kinetics (Table 2). All aerobic respiration is considered microbial, competition from root respiration here is not considered. Anaerobic respiration was represented by second-order Fe reduction. Nitrate and Mn reduction were excluded due to the relatively low concentrations in our soil. Fe reduction was included based on prior observations of microsites with redox potentials conducive to ferrihydrite reduction in *V. faba* rhizosphere soil (Fischer et al., 1989). Note that ammonium is included in both aerobic and anaerobic reactions (Table 2) solely for the purpose of balancing the equations and is not considered in model dynamics, nor was the nitrogen cycle simulated as part of this work. Fe(III) reduction causes the dissolution of Fe oxides, which mobilizes sorbed organic carbon or reduces the available surface sites for DOC sorption. The model allows both aerobic and anaerobic (i.e., DO and Fe(III) oxide reduction) respiration to occur simultaneously, with a higher rate for DO reduction. This modeling framework is consistent with the notion that both aerobic and anaerobic respiration can co-occur within soil microsites (Keiluweit et al., 2017).

Initial and boundary conditions for reactive transport. Based on our measurements, the initial condition of DO, NO_3^-, and Fe(III) oxide concentrations are 62 μmol L^{-1}, 0.15 mmol L^{-1}, and 0.1 mmol g^{-1}, respectively. As Fe^{2+} is below detection during the experiment, 1 μmol L^{-1} is assumed initially. The initial pH is 6.0. Fixed DO concentration of 75 μmol L^{-1} is applied at the boundaries.

3. Results

3.1. Empirical observations

Photosynthesis and Transpiration Rates. Plants grew in rhizoboxes inside growth chambers where they experienced simulated day and night cycles leading to an increase in photosynthetic and transpiration activity during the day and reduced rates at night. During the day photosynthetic rates were measured to be on average 13.6 μmol CO_2 m^{-2} s^{-1} whereas transpiration rates were 2.81 H_2O mol^{-2} s^{-1} (Fig. SI-4).

Rhizosphere DOC, DO, and pH/E_H. Upon root contact with the microsensors (t = 7 h) (Fig. 3a), DOC and DO concentrations as well as pH and E_H followed clear diel patterns (Fig. 3). During the day, DOC concentrations increased to ~3–6 mmol L^{-1} and declined to a baseline of ~1–1.5 mmol L^{-1} at night (Fig. 3a). Concurrently, DO concentrations declined during the day, with a minimum of ~56 μmol L^{-1} (Fig. 3b), but consistently increased during the nighttime. Similarly, E_H dropped sharply to a daytime minimum (0.39–0.36 mV) and consistently recovered to a nighttime baseline (0.41–0.42 mV) (Fig. 3c). pH reached a maximum (6.5–7.1) during the day and a minimum (6.2–6.5) at night (Fig. 3d). The daytime increases in DOC were significantly and negatively correlated with DO (R^2 = 0.16, $p < 0.05$) and E_H (R^2 = 0.42, $p < 0.01$) (Fig. 3e and f), suggesting that the rhizosphere became more reducing due to the input of root derived DOC. On the other hand, DOC concentrations showed a significant positive correlation with pH (R^2 = 0.43, $p < 0.01$) (Fig. 3g).

3.2. Simulation of diel DOC, DO and pH dynamics

Our numerical model was developed based on the initial conceptual model (Fig. 2) and constrained using soil parameters and reactions given in Tables SI-1a-c, 1 and 2. In a first step, we assessed the ability of the model to simulate our experimental data (Fig. 3) and iteratively adjusted the parameters if needed to better match the observations (Fig. 4).

DOC dynamics. In our model, DOC released by the root is directly coupled to photosynthetic rates, causing increased DOC in the rhizosphere during the day. DOC concentrations at night are drawn down due to the combination of limited root supply and DOC consumption through sorption and microbial respiration (Fig. 3a). To match the background DOC concentrations of ~1 mmol L^{-1} in the observation, we added 0.7 mM of background DOC (nonreactive) to the initial condition. The DOC supply (or exudation) rate was set to 0.048 μmol C min^{-1} for 6 h in the middle of each light period. The maximal rate was capped by C assimilation through photosynthesis (40% of measured rates) and the timing was adjusted until the best fit for the diel DOC oscillations was found. The rate parameters for respiration reactions were derived by a trial-and-error procedure to match the observations, especially pH dynamics. Our initial model included only reversible equilibrium sorption, which did not consume enough DOC to produce adequate fits (Fig. SI-5). Adding a first order irreversible reaction for DOC sorption with a rate constant of 70 mol^{-1} L^{-1} d^{-1} represented the diel variations in DOC concentrations well (R^2 = 0.4, p = 0.001) (Fig. 4a).

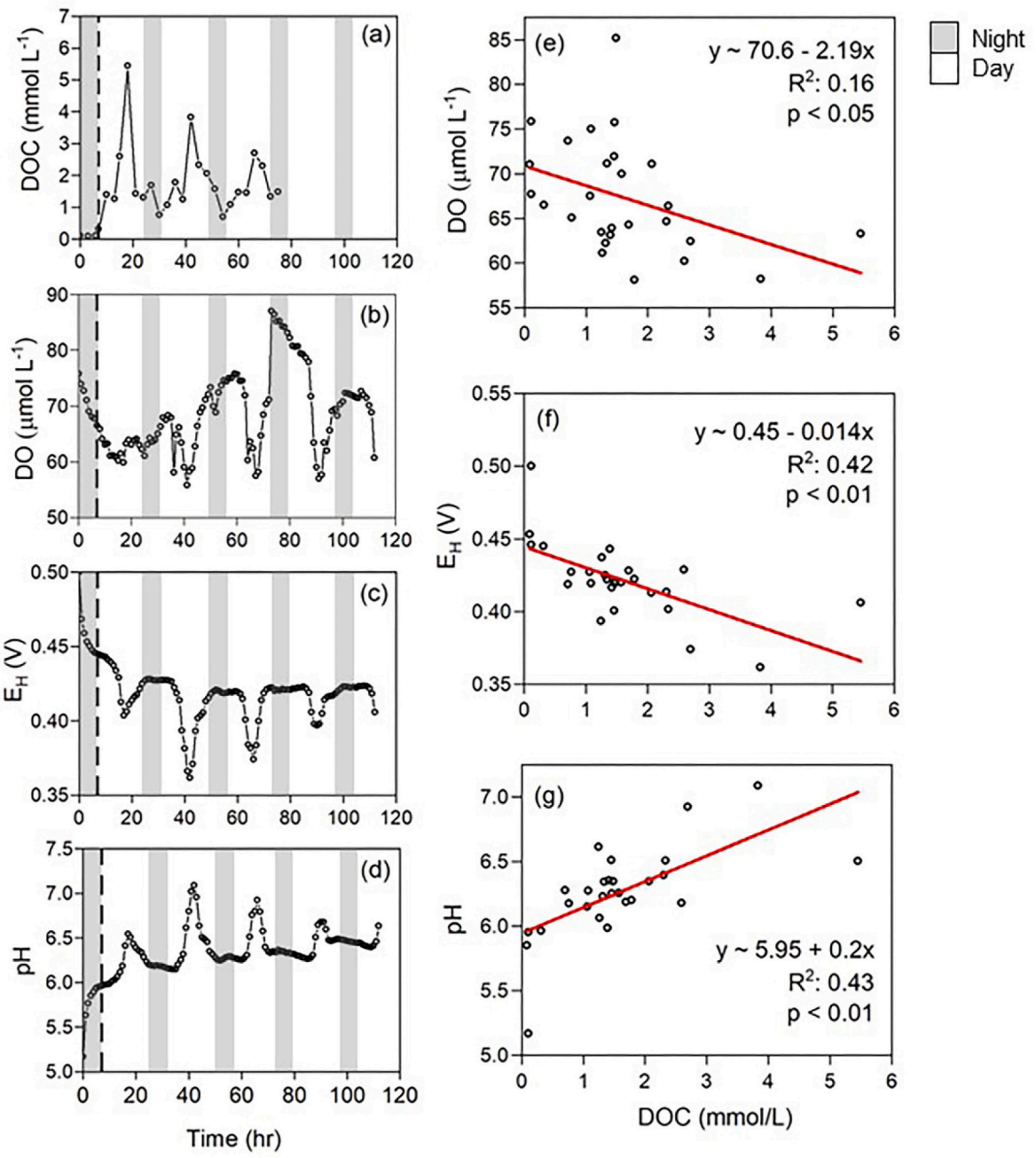

Fig. 3. Concurrent diel oscillations in rhizosphere (a) DOC concentrations (b) DO, (c) E_H, and (d) pH measured using microsensors. Correlation of DOC concentrations with (e) DO, (f) E_H and (g) pH. Shaded regions denote nighttime periods. Black dotted line denotes time of root arrival.

Redox and oxygen dynamics. Both DO and E_H show declining values during the day consistent with the possible emergence of anaerobic microsites within the rhizosphere. Because DO is easier to parameterize in a model and less prone to artifacts than E_H, we chose to focus our efforts on DO. Our initial model used a fixed 75 µmol DO L^{-1} background concentration condition along the boundary that enters the domain when water was taken up by roots, allowing background levels of DO to be transported back into the model domain. This model did not fully capture the nighttime increases in DO (Fig. 4b, blue line), when DO observations returned to background levels. In this case, the resupply of DO from the boundary by water flow is not fast enough to replenish DO consumed by aerobic respiration (reaction 2 in Table 2) in the rhizosphere. Gas phase diffusion in the unsaturated root zone soil would provide faster replenishment of background DO but is not accounted for in our model. We accounted for that by adding a constant source term of DO at the root tip to mimic this process, which improved the simulated DO dynamics (Fig. 4b, red line) after 40 h compared to the initial model (Fig. 4b, red line). The revised model resulted in outputs consistent with our observations ($R^2 = 0.35$, $p < 0.001$) (Fig. 4b, red line). Simulated DO decreased for each light period and increased during the dark period as in the observation but was only minimally affected by concurrent drying and wetting cycles in the rhizosphere driven by transpiration (Fig SI-6).

Proton balance and ensuing pH *dynamics.* The results of the simulation with the best pH performance near a root tip in the middle of the rhizobox are compared to the observations ($R_2 = 0.65$, $p < 0.001$, Fig. 4). As we observed diel increases in pH, the first processes we considered was NO_3^- absorption by the root, as this pathway has often been considered a major process for root-induced pH increase (Hinsinger

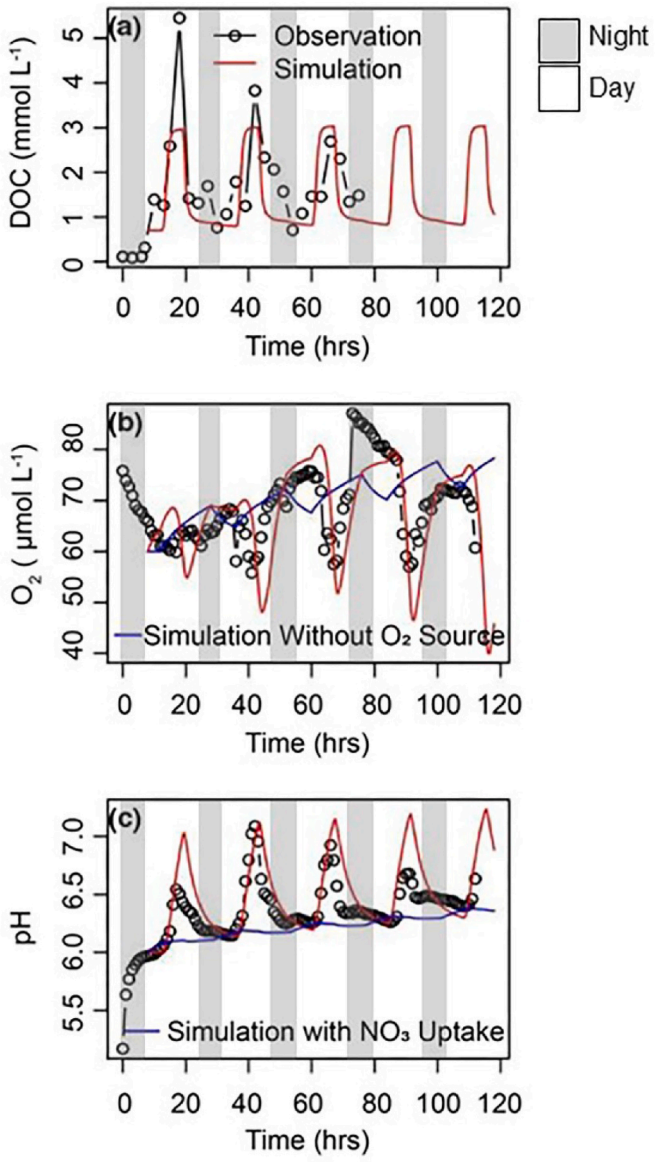

Fig. 4. Diel variations in simulated and observed (a) DOC, (b) DO, and (c) pH dynamics. Black lines denote microsensor data and red lines denote the model fit. The blue line in (b) shows simulation results without modeled DO supply at the root tip. The blue line in (c) is simulated pH change when root uptake of nitrate was included in the model. Time 0 denotes root arrival.

et al., 2003). To evaluate if this process was responsible for diel dynamics in pH, we added an active uptake of NO_3^- in the model, and HCO_3^- is released at the same rate through the root-soil interface to account for charge balance. The active uptake rate of NO_3^- is represented by a Michaelis–Menten expression. We first tested the maximum uptake rate per unit root length V_{max} and nitrate affinity constant K_m reported in (Kage, 1995) under low initial nitrate concentration conditions, which are 4.2×10^{-12} mol cm^{-1} s^{-1} and 39 µmol L^{-1}, respectively. However, this led to the complete consumption of nitrate within the first 10 h of the simulation. Reducing the rate by 3 orders of magnitude, the general increasing trend of pH (+0.4 unit at the end of the experiment) can be modeled, but not the diel dynamics (Fig. 4c, blue line). This result eliminated the possibility that the ensuing diel dynamics of the pH in this system were due to NO_3^- uptake.

With trial and error, we found that the observed pH was best explained by a second-order reaction kinetics for Fe reduction, which consumes protons (Table 2). The rate constants for Fe reduction and aerobic respiration are 7.5 mmol L^{-1} d^{-1} and 60 µmol L^{-1} d^{-1}, respectively. This falls within similar magnitude for aerobic respiration reported in microcosms spiked with organic acids in the literature, ranging from 10 µmol to 190 µmol L^{-1} d^{-1} CO_2, respectively (Van Hees et al., 2003; Li et al., 2021). Half saturation constant of DO and DOC are 20 µmol L^{-1} and 100 µmol L^{-1}, respectively. To match the peak time of DOC and pH during each light period, C was assumed to be released uniformly at the root tip during the first 6 h of the light period, which is 0.048 µmol C min^{-1}. This assumption is justifiable as it has been found that the circadian clock regulates root exudation into the rhizosphere and the peak rate of exudation tends to occur during the light periods (Watt and Evans, 1999).

3.3. Balance between exudation, sorption, and microbial utilization

We further used the model to examine the fate of root-derived C during diel cycles within the rhizosphere, specifically the balance between DOC supply (exudation) and consumption via either sorption to minerals (here ferrihydrite) or microbial respiration.

Sorption versus microbial respiration. Interestingly, the DOC released in the diel pulses greatly exceeded potential consumption via microbially-mediated terminal electron accepting processes (e.g., respiration of O_2, nitrate, Fe(III), etc.). In the model, most of the DOC cumulatively released by the root (exudation) over the course of the experiment was consumed by sorption to minerals (94%), rather than microbial respiration (6%) (Fig. 5a). To better match the observed DOC behavior, most of the sorption was modeled as irreversible, with equilibrium sorption accounting for 1.4% of total sorption. A preference for sorption over microbial respiration of organic acids aligns with empirical observations on organic acids in batch environments and in natural forest soils (Van Hees et al., 2003; Li et al., 2021).

Microbial respiration. After accounting for adsorption, the modeled DOC consumption by microbial respiration peaked during the day

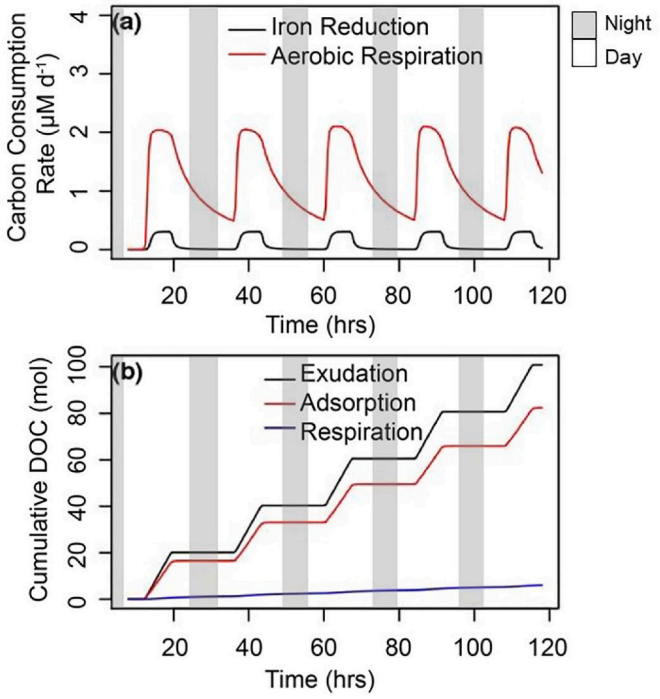

Fig. 5. Diel variations of simulated (a) DOC consumption driven by either aerobic respiration or iron reduction (anaerobic respiration) and (b) proportion of total cumulative root-derived DOC released during the simulation that was subject to either adsorption or microbial respiration (consumption). Shaded regions denote nighttime periods. Modeling started after the first dark period in the experimental data at t = 8.

(Fig. 5b), coinciding with the daytime pulse of root-derived DOC (exudation) (Fig. 5a). DOC was predominantly consumed via aerobic respiration (92.8% at the end of the simulation), with a smaller but notable contribution from microbial Fe reduction (i.e., anaerobic respiration) (7.2%) (Fig. 5a).

3.4. Dynamics of Fe-associated C in the rhizosphere

Though simulations indicated that fresh root-derived DOC (exudates) rapidly sorbed to Fe(III) oxides (Fig. 5a), DOC adsorption/desorption eventually followed diel cycles driven by equilibrium reactions (Fig. 6a): adsorption of DOC dominated during light periods; desorption occurred during dark periods. To assess what role Fe(III) oxide reduction played in the mobilization of previously sorbed carbon, we modeled changes in Fe(II) production (Fig. 6a). Small yet noticeable increases in soluble Fe(II) concentrations were modeled during the day (Fig. 6a, red line), which was in good agreement with the coinciding minima in DO concentrations (Fig. 3b). However, increased Fe(II) production did not correlate with a decrease in sorbed carbon (Fig. 6a, blue line). Finally, we examined whether mineral surface availability may have influenced the dynamics of sorbed DOC by assessing changes in the amount of total Fe(III) oxides over time. Our simulations show that the amount of Fe(III) oxide available for sorption (red line) increased during the day although the amount of sorbed carbon decreased (Fig. 6b, blue line).

4. Discussion

The eSTOMP-ROOTS model was able to reproduce the measured diel oscillations in rhizosphere DOC concentrations, redox and pH conditions well using measured plant physiological inputs and reasonable parameterization of sorption/desorption and Michaelis-Menton kinetics.

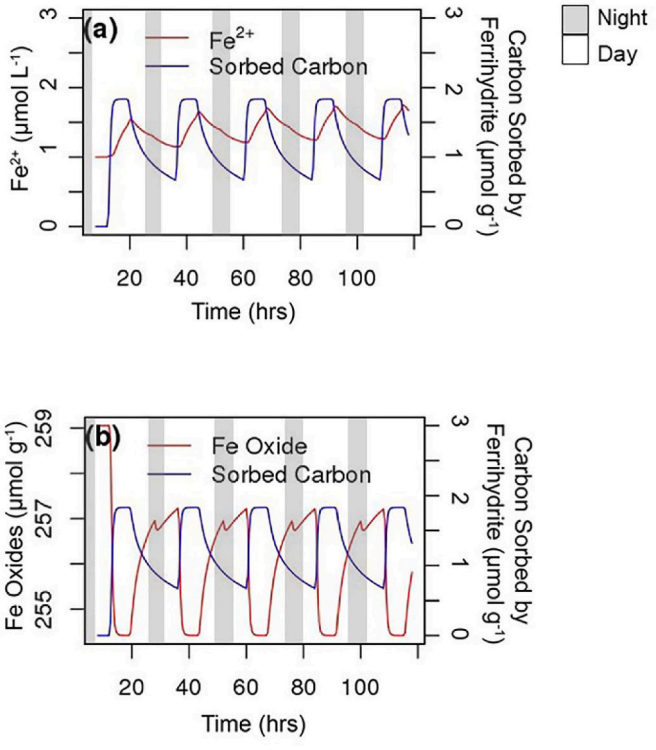

Fig. 6. Simulation of DOC sorption/desorption to Fe(III) oxides in relation to variations in (a) Fe^{2+} concentrations as a measure of Fe(III) oxide dissolution and (b) available Fe(III) oxide surface area for sorption. Both parameters yield information about the degree of reduction and oxidation causing Fe (III) oxide dissolution and precipitation, respectively. Shaded regions denote nighttime periods. Modeling started after the first dark period in the experimental data at t = 8.

4.1. Influence of diel cycles in plant activity on rhizosphere biogeochemistry

Throughout our experiments, photosynthetic and transpiration activity were highest during the day (Fig. SI-4), as were rhizosphere DOC concentrations measured by microdialysis and modeled by eSTOMP-ROOTS. Elevated DOC concentrations, in turn, coincided with sharp declines in measured DO and E_H (Fig. 3a, b, c), suggesting increased bioavailable DOC enhanced aerobic respiration and DO consumption with declines in E_H. At night, reduced photosynthesis and bioavailable DOC likely slowed microbial respiration and led to the empirically observed restoration of background DO concentrations via diffusion from the surrounding soil. This oscillation in microbial activity reflecting diel cycles has also been found around plant roots before (Herron et al., 2013). These dynamics for empirical E_H and DO data were simulated in our model but required the incorporation of a generation term for DO.

In our experiment, DO concentrations and E_H values overall remained at values (>55 μM and >0.4 V, respectively) considered oxic. However, it is possible that anaerobic microsites as previously observed (Fischer et al., 1989) remained undetected in our system. Our microelectrodes integrate DO and E_H values over 300–400 μm of soil (Luther et al., 2008), while anaerobic microsites smaller than 100 μm in diameter have been observed (Keiluweit et al., 2017). It is therefore possible that our microelectrodes averaged over an area significantly larger than individual microsites, thus only measuring a relatively subtle decline in bulk DO concentrations (and, by extension, E_H).

4.2. Integrating microsensor data into mechanistic plant-soil model to predict rhizosphere DOC dynamics

Our relatively simple conceptual model, which accounted for exudation, microbial respiration, and sorption to minerals (Fig. 2), was able to represent the measured diel dynamics in rhizosphere DOC well. Exudation was estimated based on photosynthetic rates and normalized to a root mass from the literature (Zhao et al., 2017), resulting in an emergent exudation rate of 0.053 μmol C min^{-1} g^{-1} root biomass that is in good agreement with previously reported rates of 0.17–0.35 μmol C min^{-1} g^{-1} root biomass (de Vries et al., 2019; grasses) to 0.006–0.014 μmol C min^{-1} g^{-1} root biomass (Canarini and Dijkstra, 2015; soybean and sunflower) when grown in soil environments at optimal conditions. Overall modeled rates of aerobic (Van Hees et al., 2003; Li et al., 2021) and anaerobic respiration (Tishchenko et al., 2015), as well as the ratio of aerobic versus anaerobic contributions (Keiluweit et al., 2017) are also in good agreement with previous reports.

Rhizosphere soil moisture dynamics remain a potential source of uncertainty in the model in two ways. First, without fine-scale measurements, we relied on model estimates for soil moisture dynamics based on transpiration and advective transport in the soil. This approach predicted minimal temporal variations in rhizosphere soil moisture (Figs. S1–5). Going forward, a combination of our microsensor approach with dynamic measurements of rhizosphere water dynamics (e.g., through neutron radiography, Carminati, 2013) would allow us to better constrain the hydro-biogeochemical processes that drive C cycling in the rhizosphere. For example, during the day, active selective water uptake (plant transpiration) may have the potential to lower local water content sufficiently to cause detectably higher DOC concentrations in rhizosphere porewater (Cardon and Gage, 2006; Espeleta et al., 2017). At night, when transpiration ceases and an influx of water from the surrounding bulk soil equalizes rhizosphere and bulk water potential, rhizosphere DOC concentrations may be diluted (Holder and Brown, 1980; Cardon and Gage, 2006). Second, the gaseous transport of oxygen through drained pore space is not modeled by eSTOMP-ROOTS.

Modeled O_2 transport towards the root was solely via transpiration-driven advection and was not sufficient to replenish DO concentrations at night; to match observed DO dynamics, a constant source term of DO at the root tip was required to mimic gaseous diffusion toward the root. An explicit consideration of O_2 diffusion within air-filled pores within the unsaturated soil pore space would thus be beneficial.

4.3. Limited microbial exudate consumption sets the stage for rapid sorption to Fe oxides

Although root exudates are often expected to "prime" microbial activity in rhizosphere soils, our modeling results further confirm prior assertations that minerals act as a strong control on the microbial utilization of root exudates. DOC concentrations during each daytime release, significantly exceeded, the electron equivalents in the relatively small pool of terminal electron acceptors potentially available for microbially-mediated reduction. Our model predicted that the vast majority of exudate C released by the root (94%) was promptly consumed by sorption to ferrihydrite surfaces, with only a small fraction consumed by microbes (6%). Such preferential sorption over microbial biomass incorporation of organic acids is consistent with other studies. For example, Van Hees et al., 2003 showed that citric, oxalic, and acetic acids are rapidly sorbed to mineral soils containing significant amounts of Fe and Al (oxyhydr)oxides, reducing microbial mineralization by 35–99%. More recently, Li et al. (2021) showed that more than 90% of oxalic acid added to model soils containing Fe and Al (oxyhydr)oxides was directly sorbed onto mineral surfaces, thereby escaping microbial mineralization. Other common compounds released by plant roots (e.g. sugars) likely would not behave similarly, suggesting that sorptive mineral surfaces may modulate the quantity and quality of exudates available for microbial use.

4.4. DOC is mobilized from ferrihydrite via desorption, rather than reductive dissolution

eSTOMP-ROOTS predicted episodic destabilization of sorbed organic Cover diel cycles (Fig. 6a and b). Modeled reductive dissolution of ferrihydrite did not mobilize significant amounts of previously sorbed organic C as DOC (Fig. 6a), though it is known that in other soil systems experiencing redox oscillations, reductive dissolution of Fe oxides can cause the mobilization of previously Fe-bound organic C (Barcellos et al., 2018). The model predicted that DOC mobilization from Fe(III) oxide was greatest during the night, when exudation was low and microbial DOC consumption drew down DOC concentrations. The resulting low DOC concentrations shifted the sorption-desorption equilibrium to favor desorption (Fig. 6a). The model suggests diel oscillations in sorption-desorption behavior, with sorption of fresh exudates (DOC) prevailing during the day and desorption of previously mineral-associated organic C dominating during the night.

4.5. Implications

The presented mechanistic modeling framework, coupled with high-resolution, non-invasive, rhizosphere-scale and plant physiological measurements, holds significant promise for exploring the dynamics and balance of the various microbial reactions and mineral interactions controlling transformation and storage of rhizosphere carbon in diverse soils. Our data-model integration of rhizosphere processes highlights the dynamism that can characterize the formation and disruption of mineral-organic associations in the rhizosphere. The balance of mineral (de)sorption vs. microbial consumption could be explored for multiple classes of organic compounds known to be released by roots and rhizosphere microbes. The same balance could be elucidated in soils with differential mineralogy, or around roots of diverse plants experiencing environmental conditions known to spur changes in rhizodeposition. Elevated atmospheric CO_2, climate shifts toward drought, and human land use altering nutrient availability all have the potential to alter plant allocation belowground and root physiology. A mechanistic understanding of the dominant controls over the competition and dynamic exchange between microbes and minerals for rhizosphere C will be particularly valuable for predicting where and when rhizosphere processes stabilize or destabilize C in soils.

Declaration of competing interest

The authors declare that they have no known competing financial interests or personal relationships that could have appeared to influence the work reported in this paper.

Data availability

Data will be made available on request.

Acknowledgements

The authors thank C.G. Anderson and M. McCreight for help with soil sampling and analysis and H. Mashayekhi for assistance with the DOC analysis. M. Garcia Arredondo was supported through an NSF GFRP and UMASS Smith-Spaulding Fellowship. Y. Fang and S. Yabusaki were supported by the Environmental Molecular Sciences Laboratory (EMSL) RhizoSys project. EMSL is a national scientific user facility sponsored by the Department of Energy's Office of Biological and Environmental Research, located at Pacific Northwest National Laboratory (PNNL). PNNL is operated for the DOE by Battelle Memorial Institute under contract DE-AC05-76RLO 1830. M. Keiluweit is supported through SNF Project Funding (No. 200021_213101). This work was supported by the US Department of Energy, Office of Biological and Environmental Research, Environmental System Science Program (Award Nos. DE-SC0019477 to M. Keiluweit and DE-SC0021093 and DE-SC0019142 to Z.G. Cardon).

Appendix A. Supplementary data

Supplementary data to this article can be found online at https://doi.org/10.1016/j.soilbio.2023.109097.

References

Bailey, V.L., Pries, C.H., Lajtha, K., 2019. What do we know about soil carbon destabilization? Environmental Research Letters 14 (8), 083004. https://doi.org/10.1088/1748-9326/ab2c11.

Barcellos, D., Cyle, K.T., Thompson, A., 2018. Faster redox fluctuations can lead to higher iron reduction rates in humid forest soils. Biogeochemistry 137 (3), 367–378. https://doi.org/10.1007/s10533-018-0427-0.

Brackin, R., Atkinson, B.S., Sturrock, C.J., Rasmussen, A., 2017. Roots-eye view: using microdialysis and microCT to non-destructively map root nutrient depletion and accumulation zones. Plant, Cell and Environment 40 (12), 3135–3142. https://doi.org/10.1111/pce.13072.

Calabrese, S., Porporato, A., 2019. Impact of ecohydrological fluctuations on iron-redox cycling. Soil Biology and Biochemistry 133, 188–195. https://doi.org/10.1016/j.soilbio.2019.03.013.

Canarini, A., Dijkstra, F.A., 2015. Dry-rewetting cycles regulate wheat carbon rhizodeposition, stabilization and nitrogen cycling. Soil Biology and Biochemistry 81, 195–203. https://doi.org/10.1016/j.soilbio.2014.11.014.

Cardon, Z.G., Gage, D.J., 2006. Resource exchange in the rhizosphere: molecular tools and the microbial perspective. Annual Review of Ecology Evolution and Systematics 37 (1), 459–488. https://doi.org/10.1146/annurev.ecolsys.37.091305.110207.

Carminati, A., 2013. Rhizosphere wettability decreases with root age: a problem or a strategy to increase water uptake of young roots? Front. in Plant Sci. 4 (298) https://doi.org/10.3389/fpls.2013.00298.

Carsel, R.F., Parrish, R.S., 1988. Developing joint probability distributions of soil water retention characteristics. Water Resources Research 24 (5), 755–769. https://doi.org/10.1029/WR024i005p00755.

Cheng, W., Gershenson, A., 2007. Carbon fluxes in the rhizosphere. In: The Rhizosphere. Elsevier, pp. 31–56. https://doi.org/10.1016/B978-012088775-0/50004-5.

Clemmensen, K.E., Bahr, A., Ovaskainen, O., Dahlberg, A., Ekblad, A., Wallander, H., Stenlid, J., Finlay, R.D., Wardle, D.A., Lindahl, B.D., 2013. Roots and associated

fungi drive long-term carbon sequestration in boreal forest. Science 339 (6127), 1615–1618. https://doi.org/10.1126/science.1231923.
Courchesne, F., Turmel, M.C., 2007. Extractable Al, Fe, Mn, and Si. In: Carter, M.R., Gregorich, E.G. (Eds.), Soil Sampling and Methods of Analysis, second ed. CRC, Boca Raton, FL. https://doi.org/10.1201/9781420005271.CH26.
Dai, H., Wu, B., Chen, B., Ma, B., Chu, C., 2022. Diel fluctuation of extracellular reactive oxygen species production in the rhizosphere of rice. Environ. Sci. Technol. 56 (12), 9075–9082. https://doi.org/10.1021/acs.est.2c00005.
de Vries, Williams, A., Stringer, F., Willcocks, R., McEwing, R., Langridge, H., Straathof, A.L., 2019. Changes in root-exudate-induced respiration reveal a novel mechanism through which drought affects ecosystem carbon cycling. New Phytologist 224 (1), 132–145. https://doi.org/10.1111/nph.16001.
Dennis, P.G., Miller, A.J., Hirsch, P.R., 2010. Are root exudates more important than other sources of rhizodeposits in structuring rhizosphere bacterial communities?: root exudates and rhizosphere bacteria. FEMS Microbiology Ecology 72 (3), 313–327. https://doi.org/10.1111/j.1574-6941.2010.00860.x.
Espeleta, J.F., Cardon, Z.G., Mayer, K.U., Neumann, R.B., 2017. Diel plant water use and competitive soil cation exchange interact to enhance NH4 + and K+ availability in the rhizosphere. Plant and Soil 414 (1–2), 33–51. https://doi.org/10.1007/s11104-016-3089-5.
Fang, Y., Yabusaki, S.B., Ahkami, A.H., Chen, X., Scheibe, T.D., 2019. An efficient three-dimensional rhizosphere modeling capability to study the effect of root system architecture on soil water and reactive transport. Plant and Soil 441 (1–2), 33–48. https://doi.org/10.1007/s11104-019-04068-z.
Fischer, W.R., Flessa, H., Schaller, G., 1989. PH values and redox potentials in microsites of the rhizosphere. Zeitschrift für Pflanzenernährung und Bodenkunde 152 (2), 191–195. https://doi.org/10.1002/jpln.19891520209.
Fox, P.M., Carrero, S., Anderson, C., Dewey, C., Keiluweit, M., Conrad, M., Naughton, H. R., Fendorf, S., Carroll, R., Dafflon, B., Malenda-Lawrence, H., Dwivedi, D., Gilbert, B., Christensen, J.N., Boye, K., Beutler, C., Brown, W., Newman, A., Versteeg, R., et al., 2022. Sulfur biogeochemical cycling and redox dynamics in a shale-dominated mountainous watershed. Journal of Geophysical Research: Biogeosciences 127 (6). https://doi.org/10.1029/2021JG006769.
Garcia Arredondo, M., Lawrence, C.R., Schulz, M.S., Tfaily, M.M., Kukkadapu, R., Jones, M.E., Boye, K., Keiluweit, M., 2019. Root-driven weathering impacts on mineral-organic associations in deep soils over pedogenic time scales. Geochimica et Cosmochimica Acta 263, 68–84. https://doi.org/10.1016/j.gca.2019.07.030.
Gibbs, M., 1979. A simple method for the rapid determination of iron in natural waters. Water Research 13 (3), 295–297. https://doi.org/10.1016/0043-1354(79)90209-4.
Gu, B., Schmitt, J., Chen, Z., Liang, L., McCarthy, J.F., 1995. Adsorption and desorption of different organic matter fractions on iron oxide. Geochimica et Cosmochimica Acta 59 (2), 219–229. https://doi.org/10.1016/0016-7037(94)00282-Q.
Gu, Baohua, Schmitt, Juergen, Chen, Zhihong, Liang, Liyuan, McCarthy, J.F., 1994. Adsorption and desorption of natural organic matter on iron oxide: mechanisms and models. Environ. Sci. Technol. 28 (1), 38–46. https://doi.org/10.1021/es00050a007.
Hayakawa, C., Fujii, K., Funakawa, S., Kosaki, T., 2018. Effects of sorption on biodegradation of low-molecular-weight organic acids in highly-weathered tropical soils. Geoderma 324, 109–118. https://doi.org/10.1016/j.geoderma.2018.03.014.
Herron, P.M., Gage, D.J., Pinedo, C.A., Haider, Z.K., Cardon, Z.G., Rewald 2013., B.. Front. Plant Sci. Better to light a candle than curse the darkness: illuminating spatial localization and temporal dynamics of rapid microbial growth in the rhizosphere. https://doi.org/10.3389/fpls.2013.00323.
Hinsinger, P., Plassard, C., Tang, C., Jaillard, B., 2003. Origins of root-mediated pH changes in the rhizosphere and their responses to environmental constraints: a review. Plant and Soil 248 (1/2), 43–59. https://doi.org/10.1023/A:1022371130939.
Holder, C.B., Brown, K.W., 1980. The relationship between oxygen and water uptake by roots of intact bean plants. Soil Science Society of America Journal 44 (1), 21–25. https://doi.org/10.2136/sssaj1980.03615995004400010005x.
Inselsbacher, E., Öhlund, J., Jämtgård, S., Huss-Danell, K., Näsholm, T., 2011. The potential of microdialysis to monitor organic and inorganic nitrogen compounds in soil. Soil Biology and Biochemistry 43 (6), 1321–1332. https://doi.org/10.1016/j.soilbio.2011.03.003.
Javaux, M., Schröder, T., Vanderborght, J., Vereecken, H., 2008. Use of a three-dimensional detailed modeling approach for predicting root water uptake. Vadose Zone Journal 7 (3), 1079–1088. https://doi.org/10.2136/vzj2007.0115.
Jones, D.L., Darrah, P.R., 1994. Role of root derived organic acids in the mobilization of nutrients from the rhizosphere. Plant and Soil 166 (2), 247–257. https://doi.org/10.1007/BF00008338.
Kage, H., 1995. Interaction of nitrate uptake and nitrogen fixation in faba beans. Plant and Soil 176 (2), 189–196. https://doi.org/10.1007/BF00011782.
Keiluweit, M., Bougoure, J.J., Nico, P.S., Pett-Ridge, J., Weber, P.K., Kleber, M., 2015. Mineral protection of soil carbon counteracted by root exudates. Nature Climate Change 5 (6), 588–595. https://doi.org/10.1038/nclimate2580.
Keiluweit, M., Wanzek, T., Kleber, M., Nico, P., Fendorf, S., 2017. Anaerobic microsites have an unaccounted role in soil carbon stabilization. Nature Communications 8 (1), 1771. https://doi.org/10.1038/s41467-017-01406-6.
Knott, C.M., 1990. A key for stages of development of the faba bean (Vicia faba). Annals of Applied Biology 116 (2), 391–404. https://doi.org/10.1111/j.1744-7348.1990.tb06621.x.
Kuzyakov, Y., Domanski, G., 2000. Carbon input by plants into the soil. Review. Journal of Plant Nutrition and Soil Science 163 (4), 421–431. https://doi.org/10.1002/1522-2624(200008)163:4<421::AID-JPLN421>3.0.CO;2-R.
Leitner, D., Klepsch, S., Bodner, G., Schnepf, A., 2010. A dynamic root system growth model based on L-Systems: tropisms and coupling to nutrient uptake from soil. Plant and Soil 332 (1–2), 177–192. https://doi.org/10.1007/s11104-010-0284-7.
Leitner, D., Meunier, F., Bodner, G., Javaux, M., Schnepf, A., 2014. Impact of contrasted maize root traits at flowering on water stress tolerance – a simulation study. Field Crops Research 165, 125–137. https://doi.org/10.1016/j.fcr.2014.05.009.
Li, H., Bölscher, T., Winnick, M., Tfaily, M.M., Cardon, Z.G., Keiluweit, M., 2021. Simple plant and microbial exudates destabilize mineral-associated organic matter via multiple pathways. Environ. Sci. Technol. 55 (5), 3389–3398. https://doi.org/10.1021/acs.est.0c04592.
Lo Presti, E., Badagliacca, G., Romeo, M., Monti, M., 2021. Does legume root exudation facilitate itself P uptake in intercropped wheat? Journal of Soil Science and Plant Nutrition 21 (4), 3269–3283. https://doi.org/10.1007/s42729-021-00605-x.
Luther, G.W., Glazer, B.T., Ma, S., Trouwborst, R.E., Moore, T.S., Metzger, E., Kraiya, C., Waite, T.J., Druschel, G., Sundby, B., Taillefert, M., Nuzzio, D.B., Shank, T.M., Lewis, B.L., Brendel, P.J., 2008. Use of voltammetric solid-state (micro)electrodes for studying biogeochemical processes: laboratory measurements to real time measurements with an in situ electrochemical analyzer (ISEA). Marine Chemistry 108 (3–4), 221–235. https://doi.org/10.1016/j.marchem.2007.03.002.
Marinos, R.E., Bernhardt, E.S., 2018. Soil carbon losses due to higher pH offset vegetation gains due to calcium enrichment in an acid mitigation experiment. Ecology 99 (10), 2363–2373. https://doi.org/10.1002/ecy.2478.
McDougall, B.M., Rovira, A.D., 1970. Sites of exudation of 14C-labelled compounds from wheat roots. New Phytologist 69 (4), 999–1003.
Neurath, R.A., Pett-Ridge, J., Chu-Jacoby, I., Herman, D., Whitman, T., Nico, P.S., Lipton, A.S., Kyle, J., Tfaily, M.M., Thompson, A., Firestone, M.K., 2021. Root Carbon Interaction with Soil Minerals Is Dynamic, Leaving a Legacy of Microbially Derived Residues. Environmental Science & Technology. https://doi.org/10.1021/acs.est.1c00300 acs.est.1c00300.
Nguyen, C., 2003. Rhizodeposition of organic C by plants: mechanisms and controls. Agronomie 23 (5–6), 375–396. https://doi.org/10.1051/agro:2003011.
Perley, G.A., 1939. Characteristics of the antimony electrode. Ind. Eng. Chem. Anal. Ed. 11 (6), 319–322. https://doi.org/10.1021/ac50134a008.
Rasse, D.P., Rumpel, C., Dignac, M.-F., 2005. Is soil carbon mostly root carbon? Mechanisms for a specific stabilisation. Plant and Soil 269 (1–2), 341–356. https://doi.org/10.1007/s11104-004-0907-y.
Saarnio, S., Wittenmayer, L., Merbach, W., 2004. Rhizospheric exudation of Eriophorum vaginatum L. —potential link to methanogenesis. Plant and Soil 267 (1–2), 343–355. https://doi.org/10.1007/s11104-005-0140-3.
Schmidt, M.W.I., Torn, M.S., Abiven, S., Dittmar, T., Guggenberger, G., Janssens, I.A., Kleber, M., Kögel-Knabner, I., Lehmann, J., Manning, D.A.C., Nannipieri, P., Rasse, D.P., Weiner, S., Trumbore, S.E., 2011. Persistence of soil organic matter as an ecosystem property. Nature 478 (7367), 49–56. https://doi.org/10.1038/nature10386.
Schnepf, A., Leitner, D., Landl, M., Lobet, G., Mai, T.H., Morandage, S., Sheng, C., Zörner, M., Vanderborght, J., Vereecken, H., 2018. CRootBox: a structural–functional modelling framework for root systems. Annals of Botany 121 (5), 1033–1053. https://doi.org/10.1093/aob/mcx221.
Stubbins, A., Dittmar, T., 2012. Low volume quantification of dissolved organic carbon and dissolved nitrogen: low volume analysis of DOC and TDN. Limnology and Oceanography: Methods 10 (5), 347–352. https://doi.org/10.4319/lom.2012.10.347.
Thompson, A., Chadwick, O.A., Boman, S., Chorover, J., 2006. Colloid mobilization during soil iron redox oscillations. Environ. Sci. Technol. 40 (18), 5743–5749. https://doi.org/10.1021/es061203b.
Tishchenko, V., Meile, C., Scherer, M.M., Pasakarnis, T.S., Thompson, A., 2015. Fe2+ catalyzed iron atom exchange and re-crystallization in a tropical soil. Geochimica et Cosmochimica Acta 148, 191–202. https://doi.org/10.1016/j.gca.2014.09.018.
Van Hees, P.A.W., Vinogradoff, S., Edwards, A., Godbold, D., Jones, D., 2003. Low molecular weight organic acid adsorption in forest soils: effects on soil solution concentrations and biodegradation rates. Soil Biology and Biochemistry 35 (8), 1015–1026. https://doi.org/10.1016/S0038-0717(03)00144-5.
Vepraskas, M., 2002. Redox potential measurements. Raleigh, NC: North Carolina State University. http://citeseerx.ist.psu.edu/viewdoc/download?doi=10.1.1.630.1755&rep=rep1&type=pdf. Retrieved from.
Viollier, E., Inglett, P.W., Hunter, K., Roychoudhury, A.N., Van Cappellen, P., 2000. The ferrozine method revisited: Fe(II)/Fe(III) determination in natural waters. Applied Geochemistry 15 (6), 785–790. https://doi.org/10.1016/S0883-2927(99)00097-9.
Wagai, R., Mayer, L.M., 2007. Sorptive stabilization of organic matter in soils by hydrous iron oxides. Geochimica et Cosmochimica Acta 71 (1), 25–35. https://doi.org/10.1016/j.gca.2006.08.047.
Watt, M., Evans, J.R., 1999. Linking development and determinacy with organic acid efflux from proteoid roots of white lupin grown with low phosphorus and ambient or elevated atmospheric CO2 Concentration1. Plant Physiology 120 (3), 705–716. https://doi.org/10.1104/pp.120.3.705.
Yabusaki, S.B., Fang, Y., Williams, K.H., Murray, C.J., Ward, A.L., Dayvault, R.D., Waichler, S.R., Newcomer, D.R., Spane, F.A., Long, P.E., 2011. Variably saturated flow and multicomponent biogeochemical reactive transport modeling of a uranium bioremediation field experiment. Journal of Contaminant Hydrology 126 (3–4), 271–290. https://doi.org/10.1016/j.jconhyd.2011.09.002.
Zhao, J., Sykacek, P., Bodner, G., Rewald, B., 2017. Root Traits of European Vicia faba Cultivars-Using Machine Learning to Explore Adaptations to Agroclimatic Conditions. Plant, Cell & Environment. https://doi.org/10.1111/pce.13062.